Hybrid model of a rectangular hollow cathode discharge

Z. Donkó
Department of Laser Physics, Research Institute for Solid State Physics and Optics of the Hungarian Academy of Sciences, P.O. Box 49, H-1525 Budapest, Hungary
(Received 20 October 1997)

A rectangular hollow cathode discharge was investigated by means of a two-dimensional self-consistent hybrid model combining Monte Carlo simulation of the motion of fast electrons and a fluid description of slow electrons and positive ions. Our calculations were carried out for a cold-cathode dc abnormal glow discharge in helium, operating at moderate ($\sim$1 mA/cm^2) current densities and at low ($\sim$1 mbar) pressures. The results demonstrate the existence of the hollow cathode effect in the discharge. On the other hand the energy distribution function of electrons indicates that a considerable number of fast electrons is absorbed by the anode, representing a major loss for the maintenance of the discharge. A significant fraction of primary electrons ($\approx 5-20\%$) was absorbed by the anode before they were able to produce any ions. Due to the loss of high-energy electrons at the absorbing anodes, ionization is less efficient than that in conventional (e.g., cylindrical) hollow cathodes, thereby explaining the increasing voltage—linear current density characteristics of the discharge. Backscattering of high-energy electrons from the anodes significantly affects the discharge characteristics: a backscattering coefficient of 0.2 resulted in $\approx$90% increase of the He^+ density and $\approx$60% increase of the linear current density at 2 mbar pressure and 300 V voltage. [S1063-651X(98)12206-7]

PACS number(s): 52.65.−y, 52.80.Hc

I. INTRODUCTION

Glow discharges have a very wide range of applications, including laser, spectral, and illumination light sources, surface modification, and analytical and plasma chemistry. Modeling of the discharges helps towards an understanding of their physical details and assists in optimizing their applications.

The cathode region of cold cathode glow discharges—consisting of the cathode dark space (or cathode sheath) and the negative glow—is of particular importance and interest, as the processes responsible for the self-sustainment of the discharge take place in this region. Induced by the bombardment of positive ions, metastable atoms, and ultraviolet photons, primary electrons are emitted from the cathode and are accelerated in the electric field in the cathode dark space, thereby creating electron avalanches via ionization processes. Under stationary conditions the average number of the above particles reaching the cathode (from one electron avalanche) is precisely enough to liberate a ''new'' primary electron [1].

In discharges having opposite cathode surfaces the hollow cathode effect (see, e.g., [2]) may develop. The potential well formed between the opposing cathode surfaces enables the fast electrons to ''oscillate'' between them [3–5]. Some of the electrons may cross the negative glow several times in this way significantly enhancing the ionization rate. As a consequence of this, much higher currents than those in plane-cathode discharges can be carried through the discharge. Hollow cathode discharges typically exhibit ''flat'' voltage-current characteristics, i.e., their operating voltage is almost independent of the discharge current. By virtue of their intense light radiation hollow cathode discharges have important applications—as indicated above—as spectral light sources and lasers.

In abnormal glow discharges near the cathode surface a strong and rapidly changing electric field distribution is present. The large electric field gradients and the presence of boundaries (electrodes) induce nonequilibrium effects in the motion of electrons. Thus the hydrodynamic approach, which assumes that the transport parameters of particles are exclusively determined by the *local* value of the E/n—the electric field to gas density ratio—is not a sufficiently good approximation to describe the motion of electrons in the cathode region [6,7]. The hydrodynamic approach cannot even explain the *existence* of the negative glow (created by the electrons that acquired high energy in the cathode dark space) nor can it describe the oscillating motion of electrons between opposing cathode surfaces—the basic mechanism responsible for the development of the hollow cathode effect [3]. To trace the trajectories of fast electrons in the discharge we used Monte Carlo simulation [8–14] providing a fully kinetic description of the electrons' motion.

When the electrons have lost most of their kinetic energy and their motion is dominated by diffusion in low E/n regions of the discharge, Monte Carlo simulation of their trajectories becomes less efficient. On the other hand for these ''slow'' electrons the fluid approach is sufficiently accurate. The hydrodynamic description of He^+ ions is expected to be valid for the entire discharge under the conditions considered in this study [15].

Hybrid models [16–29] combining Monte Carlo simulation and the fluid description of different species can efficiently describe dc and rf discharges in 1 or 2 dimensions. In this paper we investigate a rectangular hollow cathode discharge by means of a hybrid model in which we apply Monte Carlo simulation to trace the trajectories of fast electrons and we use the fluid description of slow electrons and helium ions.

Previous 2D hybrid models were developed for discharges with cylindrical symmetry [24–29]; such discharges can be categorized as ''longitudinal'' discharges (the current

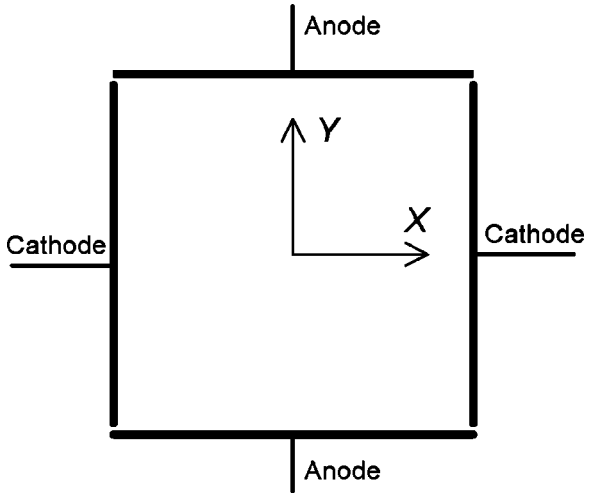

FIG. 1. Cross section of the rectangular hollow cathode discharge, indicating the Cartesian coordinate system used in the calculations. Electrodes of same polarity are separated by $D=1$ cm. The discharge is infinite in the z direction [perpendicular to the (X,Y) plane].

flows along the discharge axis). Here, we study a ''transverse'' discharge, where the current flows perpendicular to the symmetry axis of the discharge.

In Sec. II we describe the electrode configuration of the discharge, the basic assumptions and the details of the Monte Carlo and the fluid models, as well as their interfacing. The results illustrating the general behavior of the discharge are presented in Sec. III A. The effects of changing voltage and gas pressure and the effect of the backscattering of fast electrons from the anodes are shown in Secs. III B and III C, respectively. In Sec. III D the results of the calculations are compared with available published experimental data. The summary of the paper is given in Sec. IV.

II. MODEL OF THE RECTANGULAR HOLLOW CATHODE DISCHARGE

A. The discharge arrangement

The cross section of our hollow cathode discharge is shown in Fig. 1. The discharge arrangement consists of four flat electrode segments: two cathodes and two anodes face each other in a ''quadrupole'' configuration. The distance between the electrodes of the same polarity is $D=1$ cm. The product pD (where p is the gas pressure) is chosen to ensure that only the cathode dark space and the negative glow parts of the discharge develop.

The discharge is assumed to be infinite along the Z axis, which is perpendicular to the (X,Y) plane. As the current density is expected to be nonuniform on the electrode surfaces in the X and Y directions, the discharge is characterized by the *linear current density* rather than by the discharge current or current density. Linear current density expresses the current flowing along unit length of the discharge, and will be denoted here by I/L.

The electrode arrangement of the discharge shown in Fig. 1 makes it possible to develop the hollow cathode effect. In the present discharge construction, however, as the anodes are situated near to the cathodes it is highly likely that the oscillating motion of fast electrons is partially suppressed as the fast electrons can be absorbed at the anodes — especially at lower pressures.

It is mentioned that a discharge with similar electrode arrangement has already been investigated experimentally and was shown to have switching capability, controllable by a longitudinal magnetic field [30]. Also a similar discharge construction with concave electrode surfaces has been applied as a pumping source for metal ion lasers, at considerably higher current densities; see, e.g., [31].

B. Basic assumptions

In the model of the discharge cathode sputtering and gas heating are neglected because of the relatively low (≈ 1 mA/cm^2) current densities. The gas temperature is taken to be 300 K; volume recombination is neglected due to the low gas pressure.

In helium discharges the metastable atoms generally influence the electron energy distribution. This effect is most pronounced in the positive column of glow discharges and in the $0 \leqslant \varepsilon \leqslant 25$ eV range of electron energy [32]. Metastable atoms may also change the ionization rate in the discharge by electron impact ionization from the metastable states and by metastable-metastable collisions. However, in the cathode region—where electrons with energy of several hundred electronvolts are present—the effect of metastable atoms either on the electron energy distribution or the ionization balance is expected to be less important. Thus, although the metastables were found to influence some of the plasma paameters in helium discharges (e.g., plasma density, bulk electron energy) [33,34], we ignore their effects in our calculations.

We assume that secondary electron emission from the cathode is caused solely by the impact of positive ions; the secondary electron emission coefficient is chosen to be $\gamma = 0.3$.

The cathode potential is always fixed to be zero and the anode potential is equal to the discharge voltage. No account was taken of any external electrical circuit in our simulations. The density of particles on the surface of the electrodes was taken to be zero.

In most of our studies the anodes are considered to be perfect absorbers of electrons. In Sec. III C, however, we illustrate the effect on the discharge characteristics of the backscattering of fast electrons from the anode.

C. Monte Carlo model of fast electrons

The source functions of ions $S_i(x,y)$ and slow electrons $S_e(x,y)$ for a given electric field configuration are obtained from the Monte Carlo simulation of the fast electrons' motion. The primary electrons emitted from the cathode and their secondaries produced in ionizing collisions are traced in three-dimensional space until they are absorbed by one of the anodes or are no longer capable of producing any additional ions.

The initial energy of the electrons leaving the cathode was chosen to be 10 eV, their initial velocity was set perpendicular to the cathode surface.

The $\mathbf{r}(t)$ trajectory of electrons between successive collisions was followed by direct integration of their equation of motion:

$$m\frac{d^2\mathbf{r}}{dt^2}=e\mathbf{E}, \tag{1}$$

where m and e are the mass and the charge of electrons, respectively, and $\mathbf{E}$ is the electric field. The free path of electrons is assigned randomly in the Monte Carlo simulation. The position of the next collision is obtained from

$$\int_{s_0}^{s_1} n\sigma(\varepsilon(s))ds=-\ln(1-R_{01}), \tag{2}$$

where s_0 is the position of the last collision and s_1 is the position of the next collision measured on the curvilinear abscissa s, n is the background gas density, σ is the sum of cross sections of all possible elementary processes, ε is the kinetic energy of the electron, and R_{01} is a random number having a uniform distribution in the [0,1) interval (see, e.g., [9]). In the simulation Eqs. (1) and (2) are integrated simultaneously along the trajectory of the electron. Having reached the position of the next collision the electron undergoes scattering. The type of elementary process that actually occurs is chosen randomly, taking into account the values of cross sections of different processes at the given energy of the electron.

In the Monte Carlo simulation of fast electrons we took into account their elastic scattering from helium atoms, electron impact excitation, and ionization of helium atoms. The cross sections of these elementary processes were taken from Ref. [35]. The elastic scattering is anisotropic, assuming the following form for the $\sigma(\varepsilon,\chi)$ differential cross section [18,36,37]:

$$\frac{\sigma(\varepsilon,\chi)}{\sigma(\varepsilon)}=\frac{\varepsilon}{4\pi[1+\varepsilon\,\sin^2(\chi/2)]\ln(1+\varepsilon)}. \tag{3}$$

The scattering angle χ is calculated by setting the cumulative distribution function of Eq. (3) equal to a random number uniformly distributed in the [0,1) interval (see, e.g., [36]).

In the electron impact excitation process the electron loses a randomly chosen energy between the energy of the first excited level and the ionization energy of the gas atom (or between the first excited level and the actual electron energy, if the latter is less than the ionization potential). In the ionization process the energy of the ejected (ε_1) and the scattered (ε_2) electrons is partitioned in accordance with [38,39]:

$$\varepsilon_1=\omega\,\tan\left[R_{01}\,\arctan\left(\frac{\varepsilon-\varepsilon_i}{2\omega}\right)\right], \tag{4}$$

$$\varepsilon_2=\varepsilon-\varepsilon_i-\varepsilon_1, \tag{5}$$

where ε is the energy of the electron before the collision, ε_i is the ionization potential of helium, R_{01} is a random number having a uniform distribution in the [0,1) interval, and ω is a parameter characteristic for the given gas—for helium we use $\omega=15$ [38,39]. In the ionization process the velocity vectors of the incoming, the scattered, and the ejected electrons lie in the same plane. The velocity vectors of the scattered and the ejected electrons are perpendicular to each other [9]. The χ_1 and χ_2 scattering angles (measured with respect to the direction of velocity of the incoming electron) are found from (e.g., [9])

$$\cos\,\chi_1=\left(\frac{\varepsilon_1}{\varepsilon-\varepsilon_i}\right)^{1/2}, \tag{6}$$

$$\cos\,\chi_2=\left(\frac{\varepsilon_2}{\varepsilon-\varepsilon_i}\right)^{1/2}. \tag{7}$$

The azimuthal angle of the scattered electron is chosen randomly between 0 and 2π for all collision processes.

The $S_i(x,y)$ ionization source function is accumulated from the individual ionization processes. The electrons are transferred to the slow electron group [through the $S_e(x,y)$ source function] when their (kinetic+potential) energy falls below the ionization potential of helium. Here the potential energy is considered to be the difference between the maximum value of the potential in the discharge and the potential at the actual position of the electron.

D. Fluid model of slow electrons and positive ions

The fundamental variables of the fluid model are the electron density n_e, the positive ion density n_i, and the electric potential V. These quantities are functions of the Cartesian coordinates x and y (see Fig. 1). The fluid model consists of the continuity equations of electrons and ions and the Poisson equation:

$$\frac{\partial n_e}{\partial t}+\nabla(n_e\mathbf{v}_e)=S_e, \tag{8}$$

$$\frac{\partial n_i}{\partial t}+\nabla(n_e\mathbf{v}_i)=S_i, \tag{9}$$

$$\triangle V=-\frac{e}{\epsilon_0}(n_i-n_e), \tag{10}$$

where $\mathbf{v}_e$ and $\mathbf{v}_i$ are the mean velocities and S_e and S_i are the source functions of slow electrons and ions, respectively, e is the elementary charge, and ϵ_0 is the permittivity of free space. The mean velocities $\mathbf{v}_e$ and $\mathbf{v}_i$ are calculated from the momentum balance equations for electrons and ions:

$$\boldsymbol{\phi}_e=n_e\mathbf{v}_e=-n_e\mu_e\mathbf{E}-\nabla(n_eD_e), \tag{11}$$

$$\boldsymbol{\phi}_i=n_i\mathbf{v}_i=n_i\mu_i\mathbf{E}-\nabla(n_iD_i), \tag{12}$$

where $\mu_{e(i)}$ and $D_{e(i)}$ are the mobility and diffusion coefficients of electrons (ions). The diffusion coefficient of He^+ ions in helium is $D_i=410/p$ cm^2 s^{-1} (with p given in Torr) [40]; the mobility of electrons in helium is $\mu_e=10^6/p$ cm^2 V^{-1} s^{-1} [41]. The diffusion coefficient of electrons was chosen to be $D_e=10^6/p$ cm^2 s^{-1}, resulting in a fixed 1 eV characteristic energy of slow electrons [24–29]. The mobility of He^+ ions in helium was taken from Ref. [41]:

$$\mu_i = \frac{8\times10^3}{p}\left(1-8\times10^{-3}\frac{E}{p}\right)\ \mathrm{cm^2\ V^{-1}\ s^{-1}} \qquad (13)$$

for $E/p \leqslant 25$ V cm^{-1} Torr^{-1}, and

$$\mu_i = \frac{4.1\times10^4}{p}\left(\frac{E}{p}\right)^{-1/2}\left[1-27.44\left(\frac{E}{p}\right)^{-3/2}\right]\ \mathrm{cm^2\ V^{-1}\ s^{-1}} \qquad (14)$$

for $E/p > 25$ V cm^{-1} Torr^{-1}, with p given in Torr, and E given in V cm^{-1}.

In the fluid model the principal variables (n_e, n_i, and V) are defined on a grid. In the present calculations a uniform, rectangular grid of size 29×29 is used. However, due to the symmetry of the discharge, the fluid equations were solved on a smaller, 15×15, grid covering one quadrant of the discharge.

The electron and ion continuity equations are solved together with the Poisson equation by applying an implicit integration scheme [24–29]. The implicit method has the advantage of enabling a considerably longer integration time step compared with explicit integration schemes (where the continuity and Poisson equations are solved consecutively, in an iterative cycle). The numerical solution of the fluid model is based on the discretization of Eqs. (8)–(12) and the use of an exponential scheme representation of the fluxes [42]. A detailed description of the numerical method can be found in previous works [24–29].

E. Interfacing of the models

In hybrid simulations of dc discharges the fluid and Monte Carlo models are solved in an iterative way until the stationary state of the discharge is reached. In the first step of the iterations the fluid model is solved for an ''initial'' electric field distribution.

To ensure that the discharge is self-maintained, electron multiplication (M) must fulfill $M > M_0$, where M_0 satisfies the self-maintenance criterion of the discharge:

$$(M_0-1)\gamma = 1. \qquad (15)$$

Since M for the ''geometrical'' electric field distribution was usually less than needed to initiate self-sustained discharge, we assumed an initial ion density of the order of 10^9 cm^{-3}. The distortion of the field due to this initial ion density increased M to above the minimum necessary value (M_0).

In the Monte Carlo simulation the fast electrons are traced in the electric field distribution obtained from the fluid model. The spatial distribution of the electron flux emitted from the cathode is set to be proportional to the spatial distribution of the ion flux reaching the cathode (known from the solution of the fluid model).

After completing the Monte Carlo simulation cycle of a given number of primary electrons and their secondaries, the source functions were normalized by considering the actual value of the I/L linear current density (calculated in the previous fluid cycle):

$$S(x,y) = \frac{1}{e(1+1/\gamma)\triangle x \triangle y}\left(\frac{I}{L}\right)\frac{N_{xy}}{N_0}, \qquad (16)$$

where $\triangle x$ and $\triangle y$ are the divisions of the grid in the X and Y directions, N_{xy} is the number of ions (slow electrons) created in the volume element around x and y due to the emission of N_0 primary electrons from the cathode.

The source functions $S_i(x,y)$ and $S_e(x,y)$ served as input of the fluid model. Iteration of the fluid and Monte Carlo models was repeated until a converged solution was found.

The typical integration time step in the fluid model was of the order of 10 ns; the Monte Carlo part was usually run after 100 steps in the fluid model. Typically 1000 primary electrons and their secondaries were traced in the Monte Carlo procedure. Between consecutive time steps in the fluid model the $S_i(x,y)$ and $S_e(x,y)$ source functions were rescaled on the basis of the linear current density obtained at the last time step. In this way the changes in the *magnitude* of the source functions, corresponding to the change of the discharge current were taken into account. On the other hand, the ''shapes'' of the source functions—which depend on the potential distribution—remained unchanged between consecutive Monte Carlo cycles.

It is noted that the Monte Carlo simulation of ≈ 1000 primary electrons results in quite noisy source functions in two dimensions. As a consequence of this, the linear current density plotted against time also exhibits fluctuations even after the time of convergence. However, these fluctuations are much lower in magnitude than those of the source functions since the particle densities are obtained from time integration of the source functions.

Having obtained the converged value of the linear current density, the Monte Carlo simulation was run once more for 2×10^5 primary electrons to obtain sufficiently smooth two-dimensional source functions.

The calculations were carried out on a Pentium/133 personal computer. It took typically 1 day of run time to reach the converged solution for one set of discharge conditions.

F. Calculated quantities

The hybrid discharge model makes it possible to calculate several discharge parameters starting from the set of input data consisting of ''material'' constants, viz., cross sections, mobility and diffusion coefficients; and discharge conditions, viz., gas pressure and voltage.

The fluid model provides the potential distribution over the cross section of the discharge as well as the slow electron and positive ion densities. The fluxes of these particles, the electric field distribution, and the linear current density are also obtained from the fluid model.

The Monte Carlo simulation allows us to determine the energy distribution of fast electrons, the source functions of slow electrons, and ions and provides information about the statistics of ionizations as follows.

The electron avalanches that build up by the multiplication process of primary electrons (emitted from the cathode) can be characterized by the number of ions (k) created in the avalanches. Using Monte Carlo simulation of the fast electrons, the $P(k)$ statistical distribution of the number of ions created in the avalanches can be determined. The mean of the $P(k)$ distribution gives the average number of ions created for each cathode emitted electron, thus it is related to M by

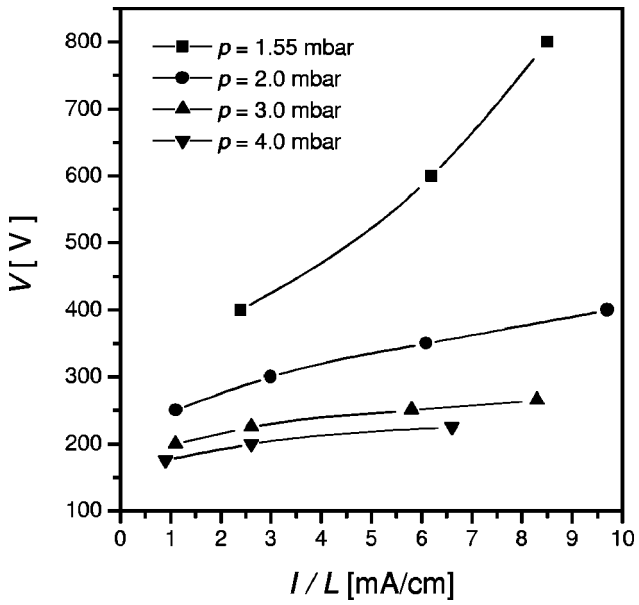

FIG. 2. Discharge voltage as a function of linear current density for different gas pressures.

$$M-1=\sum kP(k). \tag{17}$$

III. RESULTS

In this section the results of the calculations are presented. First the electrical characteristics of the discharge are shown. To illustrate the general behavior of the discharge several discharge characteristics (obtained from the Monte Carlo and the fluid model) are presented for a given set of fixed operating conditions. Following this, the dependence of some of the discharge characteristics on the discharge voltage (at constant pressure) and on the pressure (at constant linear current density) is illustrated. The effect of the backscattering of fast electrons from the anode surfaces is briefly discussed at the end of the section.

Figure 2 shows the calculated electrical characteristics of the rectangular hollow cathode discharge for different values of the helium gas pressure. The slope of the voltage-linear current density curves is higher than that of conventional hollow cathode discharges. Let us recall that in conventional (e.g., cylindrical) hollow cathode discharges the voltage is known to remain approximately constant with increasing current. The flat voltage-current curve of those discharges is due to the very efficient ion production under conditions of hollow cathode effect (see, e.g., [2]). The results presented further on show that the hollow cathode effect exists in our discharge, but there is also an increasing loss of fast electrons at the anodes with decreasing pressure.

Our calculations were carried out for linear current densities ranging from 1 mA/cm up to 10 mA/cm, for which the voltage was between 175 and 800 V, depending on the gas pressure.

A. General behavior of the discharge

All the characteristics illustrating the general behavior of the investigated hollow cathode discharge throughout Sec. III A are shown for $p=2$ mbar pressure and $V=300$ V voltage.

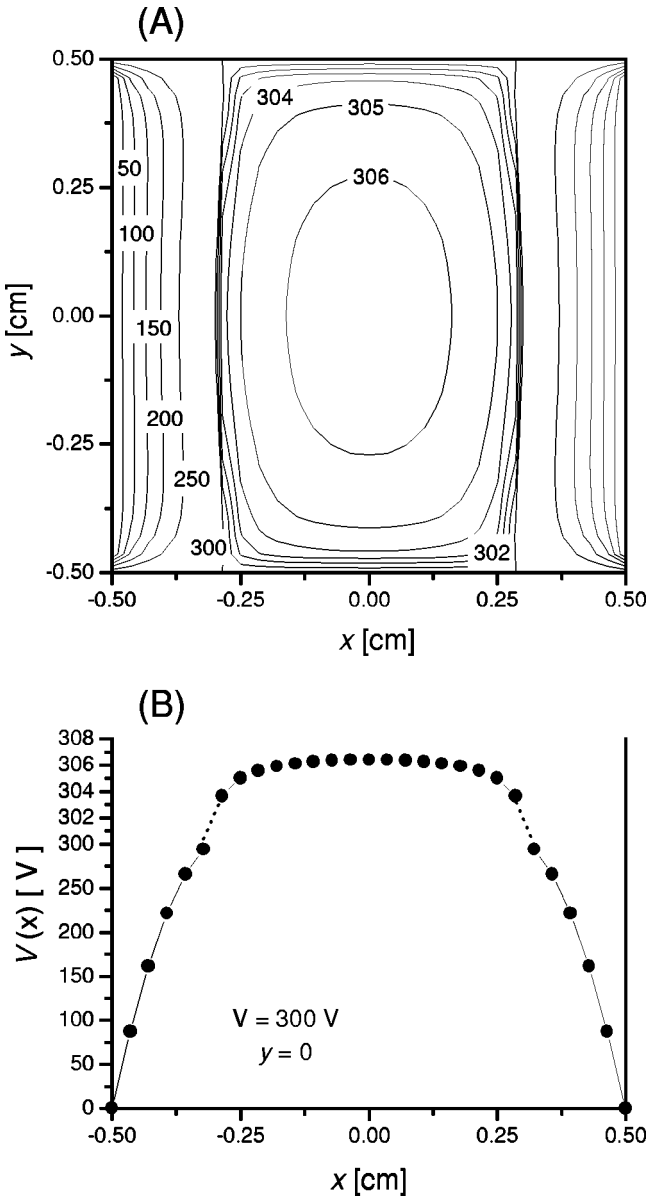

FIG. 3. (a) Potential distribution in the cross section of the rectangular hollow cathode discharge for $p=2$ mbar and $V=300$ V. (Data are given in volts.) (b) Potential distribution along the X axis. (Note that the scale is changed above 300 V.)

The potential distribution in the cross section of the discharge is plotted in Fig. 3(a); Fig. 3(b) shows the potential distribution along the X axis. In the middle part of the discharge, filled by the negative glow, we observe a plasma potential which is ≈ 6 V higher than the anode potential. The potential distribution formed in the discharge ensures that those ions not necessary to maintain the discharge are directed towards the anodes. The flux of He^+ ions to the anodes was, in fact, found to be comparable to the ion flux to the cathode. This is illustrated in Fig. 4, which displays the spatial distribution of the He^+ flux to the electrodes. Both the fluxes to the cathode and anode peak at the middle of the electrodes. It can also be seen that whereas the ion flux to the cathode has a quite broad distribution, the flux to the anode is concentrated near the middle part of the discharge as the ions are flowing to the anode only from the negative glow. The peak value of the ion flux to the anode is $\approx 40\%$ of the

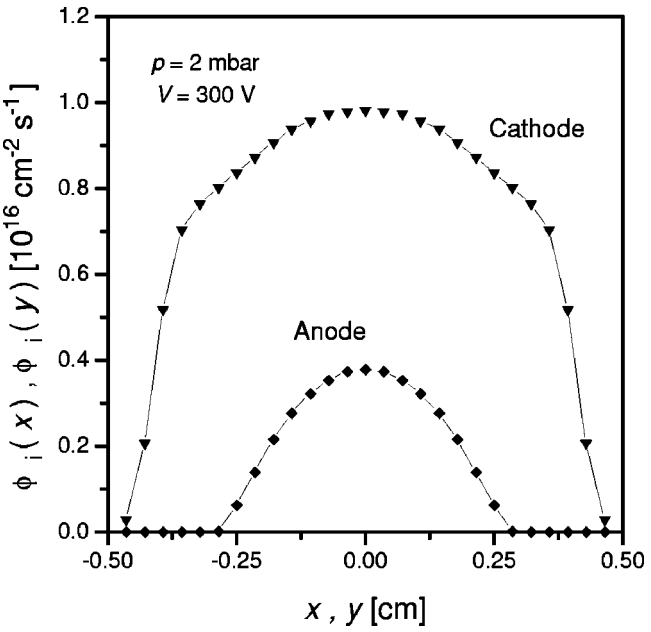

FIG. 4. Flux of He^+ ions to the cathodes $[\phi_i(y)]$ and to the anodes $[\phi_i(x)]$ for $p=2$ mbar and $V=300$ V.

ion flux to the cathode for the given discharge conditions.

A two-dimensional plot of the He^+ ion density is shown in Fig. 5(a). The $n_i(x,y)$ distribution peaks at the axis of the discharge. The formation of cathode sheaths can clearly be seen in Fig. 5(b), where the $n_i(x)$ ion and $n_e(x)$ slow electron concentrations are plotted along the X axis. In the vicinity of the cathode the positive space charge is dominant; further away from the cathode the concentration of He^+ ions and slow electrons becomes nearly equal. In the central part of the discharge a quasineutral plasma is formed with typical charged particle concentration of the order of 10^{11} cm^{-3}, corresponding to a degree of ionization between 10^{-6} and 10^{-5}.

Figure 6 illustrates the electric field distributions along the X and Y axes of the discharge. Between the midpoints of the cathodes (i.e., along the X axis; see Fig. 6) the field distribution is characteristic of a plane-parallel hollow cathode discharge [2]; between the midpoints of the anodes an electric field distribution of similar shape is found. However, the magnitude of the field in this direction $[E(y)]$ near the electrodes is ≈ 25 times less than that of the field in the direction connecting the midpoints of the cathodes $[E(x)]$. The sheaths formed at the anodes are also much shorter than those at the cathodes. The former attract the ions that are not necessary for maintaining the discharge towards the anodes and repel the electrons, thereby leading to an increase in the electron density in the negative glow.

The $S_i(x,y)$ and $S_e(x,y)$ source functions of ions and slow electrons are displayed in Figs. 7(a) and (b), respectively; Fig. 7(c) shows the source functions along the X axis. The ionization source has a quite broad and flat maximum in the central region of the discharge. The source function of slow electrons differs from zero only in the negative glow part of the discharge and has a sharp rise at the cathode dark space–negative glow boundary. In the range of parameters studied the typical ionization rate in the discharge is of the order of 10^{16} cm^{-3} s^{-1}.

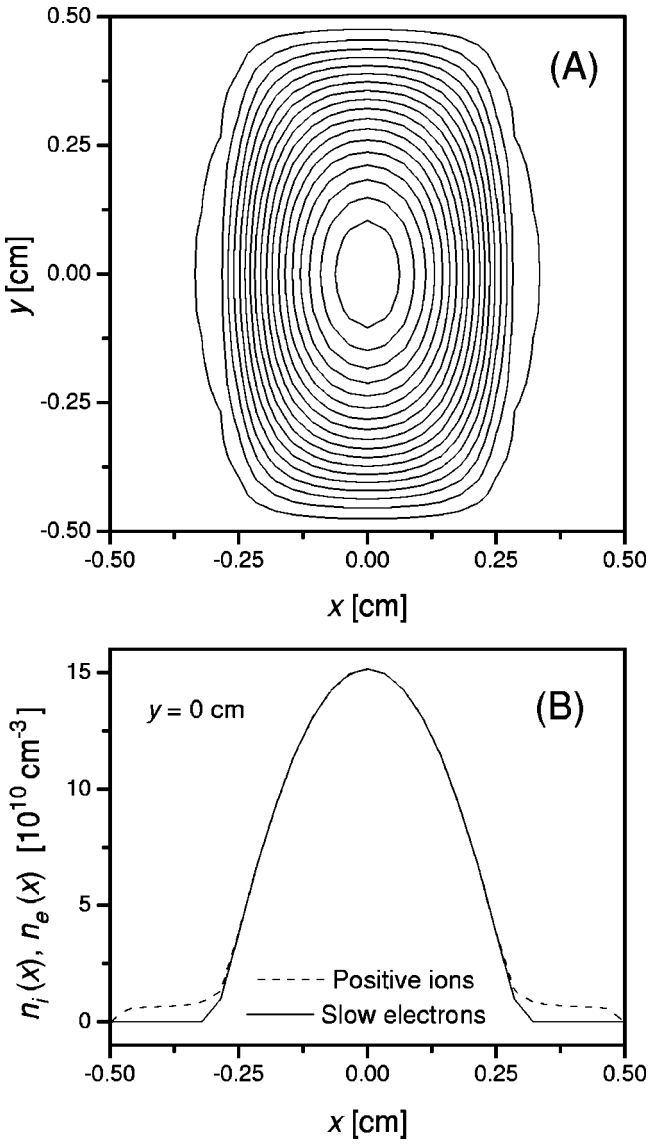

FIG. 5. (a) Two-dimensional density distribution of He^+ ions. The distance of contour lines corresponds to 10^{10} cm^{-3} change of $n_i(x,y)$. (b) Density of He^+ ions and slow electrons along the X axis ($p=2$ mbar, $V=300$ V)

The $f(\varepsilon)$ energy distribution function of high-energy ($\varepsilon > \varepsilon_i = 24.6$ eV) electrons absorbed by the anode—obtained from their Monte Carlo simulation—is plotted in Fig. 8(a). The energy distribution shows a significant loss of high-energy electrons similarly to that in obstructed discharges [43] and a glow discharge applied as an ion source [27,29].

Figure 8(b) displays the $P(k)$ distribution (ionization statistics) defined in Sec. II F. An important quantity in characterizing discharges with increased losses is $P(k=0)$: the probability that a primary electron is absorbed by the anode without producing any ions. Our data indicate that $\approx 14\%$ of the primary electrons are lost at the anode (at the given set of discharge conditions: $V=300$ V and $p=2$ mbar). Furthermore the highest value of the $P(k)$ distribution is found at $k=0$, which was rather unexpected and clearly indicates the effect of closely placed cathode and anode electrodes.

The data shown in Fig. 9 give evidence for the presence of hollow cathode effect in the discharge. The $S_i(x)$ ioniza-

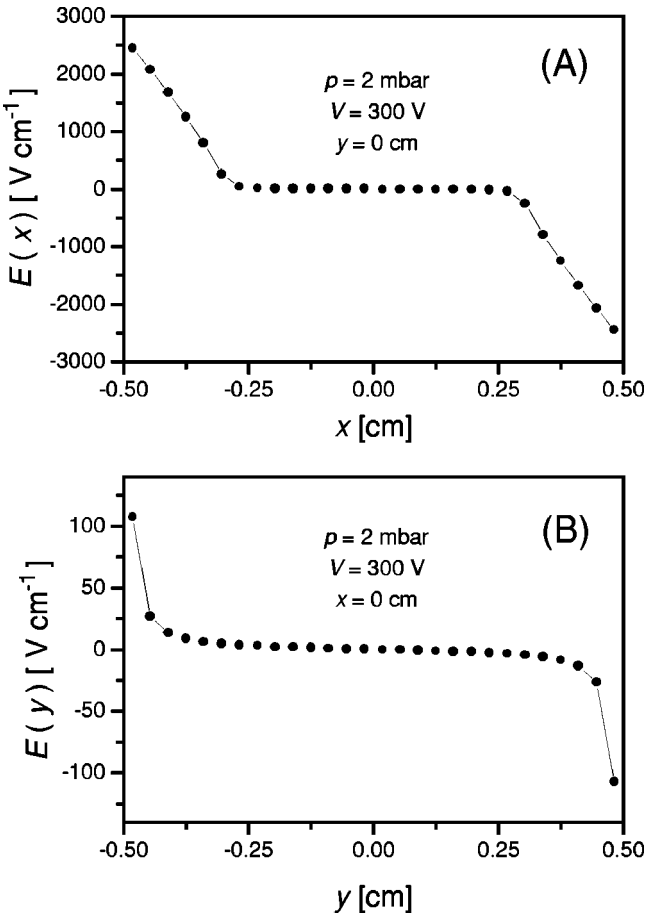

FIG. 6. Electric field distribution along the X axis (a) and the Y axis (b) of the discharge, for $p=2$ mbar and $V=300$ V.

tion source function shown in Fig. 9 is composed of two source functions corresponding to the electron avalanches starting from the ''left'' and ''right'' cathodes. It can clearly be seen that these two source functions overlap considerably, the electron avalanches starting from one of the cathodes contribute to the ion production even in the sheath of the opposite cathode.

It is mentioned that due to the significant positive ion flux to the anode, ''primary'' electrons also originate from the anodes. The anode-emitted electrons cannot, however, acquire high enough energy to ionize the gas and to multiply. Thus, their only effect is a slight increase in the electron density in the negative glow. After having checked this, we neglected the electron emission process from the anodes.

B. Effect of discharge voltage and gas pressure

In this section first we investigate the effect of changing discharge voltage at a constant pressure of 2 mbar. In Fig. 10(a) the electron multiplication is plotted as a function of voltage. With increasing voltage M increases well above M_0, the minimum multiplication necessary for the maintenance of the discharge [see Eq. (15)]. As a consequence of this, the fraction of ions reaching the anode increases from $\approx$12% at 250 V to $\approx$29% at 400 V. The extrapolation of the $M(V)$ function towards voltages lower than 250 V indicates that $M>M_0$ holds even for 200 V. Nevertheless, it was not possible to reach stationary state of the discharge even at a voltage of 225 V.

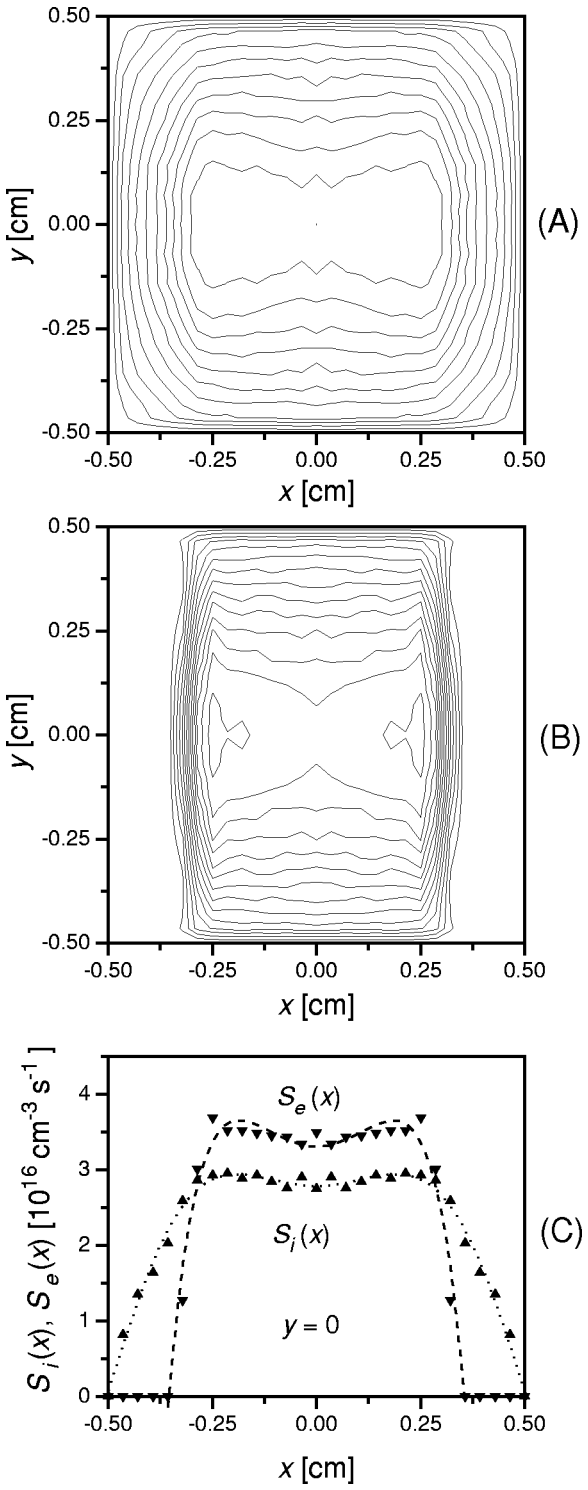

FIG. 7. Source function of He^+ ions (a) and slow electrons (b) for $p=2$ mbar and $V=300$ V. The distance of contour lines corresponds to 2.5×10^{15} cm^{-3} s^{-1} change of the $S_i(x,y)$ and $S_e(x,y)$ source functions. (c) The $S_i(x)$ and $S_e(x)$ source functions on the X axis.

In Figs. 10(b) and 10(c) the $S_i(x)$ ionization source function and the $n_i(x)$ ion density along the X axis are shown for different values of the discharge voltage. With increasing voltage both S_i and n_i exhibit a significant increase, accompanied by a decrease in the length of the cathode sheath and an increase in the linear current density (see Fig. 2).

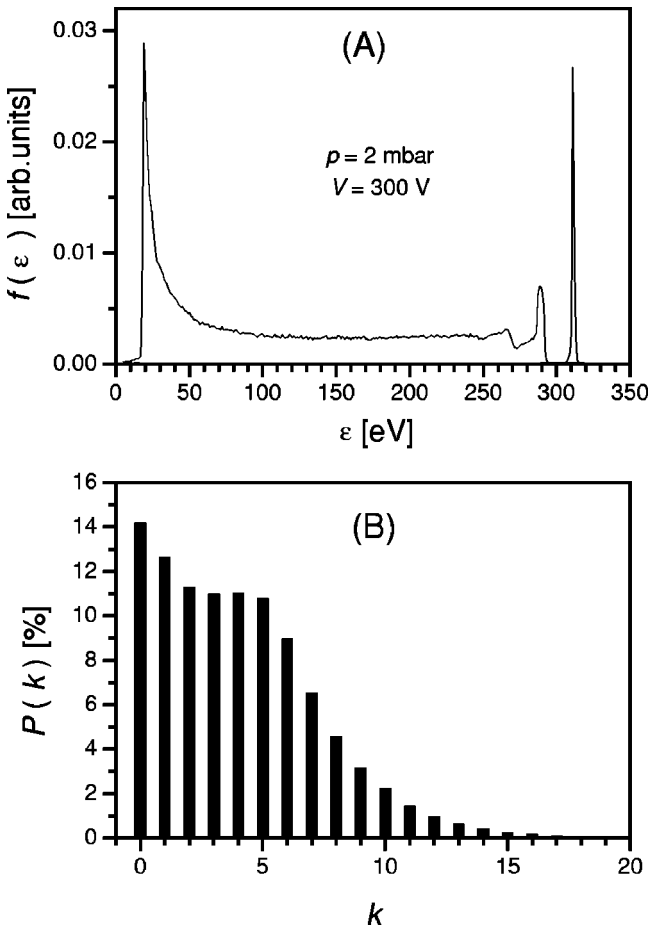

FIG. 8. (a) Energy distribution of fast ($\varepsilon > \varepsilon_i = 24.6$ eV) electrons absorbed by the anode. (b) Statistical distribution of the number of ions created in electron avalanches ($p = 2$ mbar and $V = 300$ V).

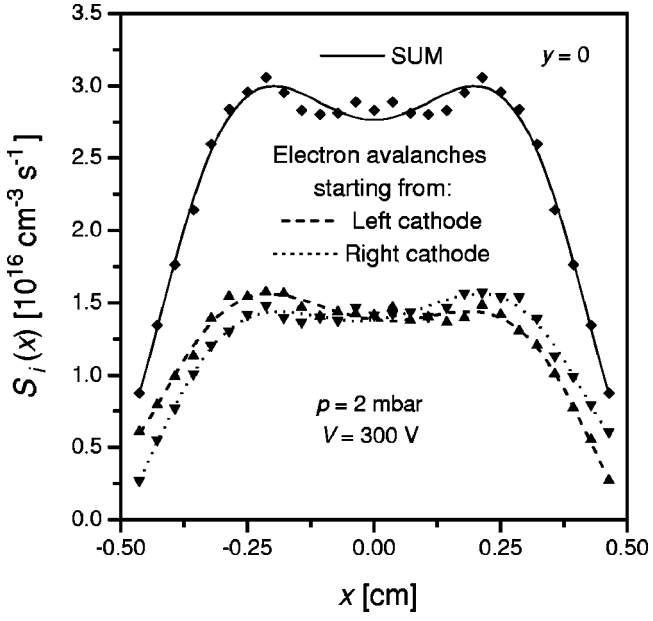

FIG. 9. Ionization source function $S_i(x)$ (on the X axis) plotted by the solid line is the sum of source functions corresponding to electron avalanches starting from the ''left'' and ''right'' cathodes.

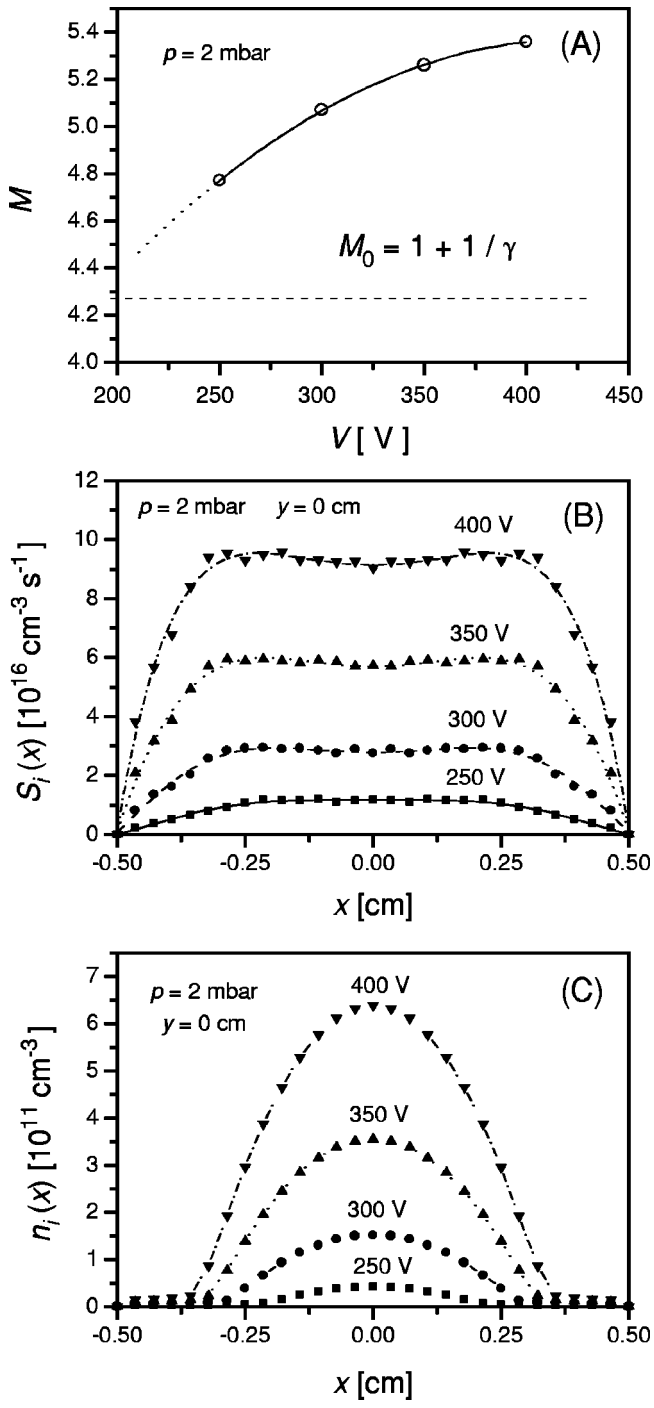

FIG. 10. Multiplication M of electrons (a), ionization source function $S_i(x)$ (b) and He^+ density $n_i(x)$ (c) for different values of the discharge voltage, at constant pressure of $p = 2$ mbar.

The effect of the changing pressure on the $S_i(x)$ and $n_i(x)$ functions at constant linear current density of 6 mA/cm is shown in Figs. 11(a) and 11(b), respectively. At the highest pressure investigated the $S_i(x)$ function exhibits two peaks, corresponding to the electron avalanches starting from the ''left'' and ''right'' cathodes. With decreasing pressure, as we approach the region of the hollow cathode effect, the ionization source becomes gradually more uniform in the central region of the discharge. The density n_i of He^+ ions along the X axis of the discharge always peaks at $x = 0$. The peak value of n_i decreases by about a factor of 5 as the

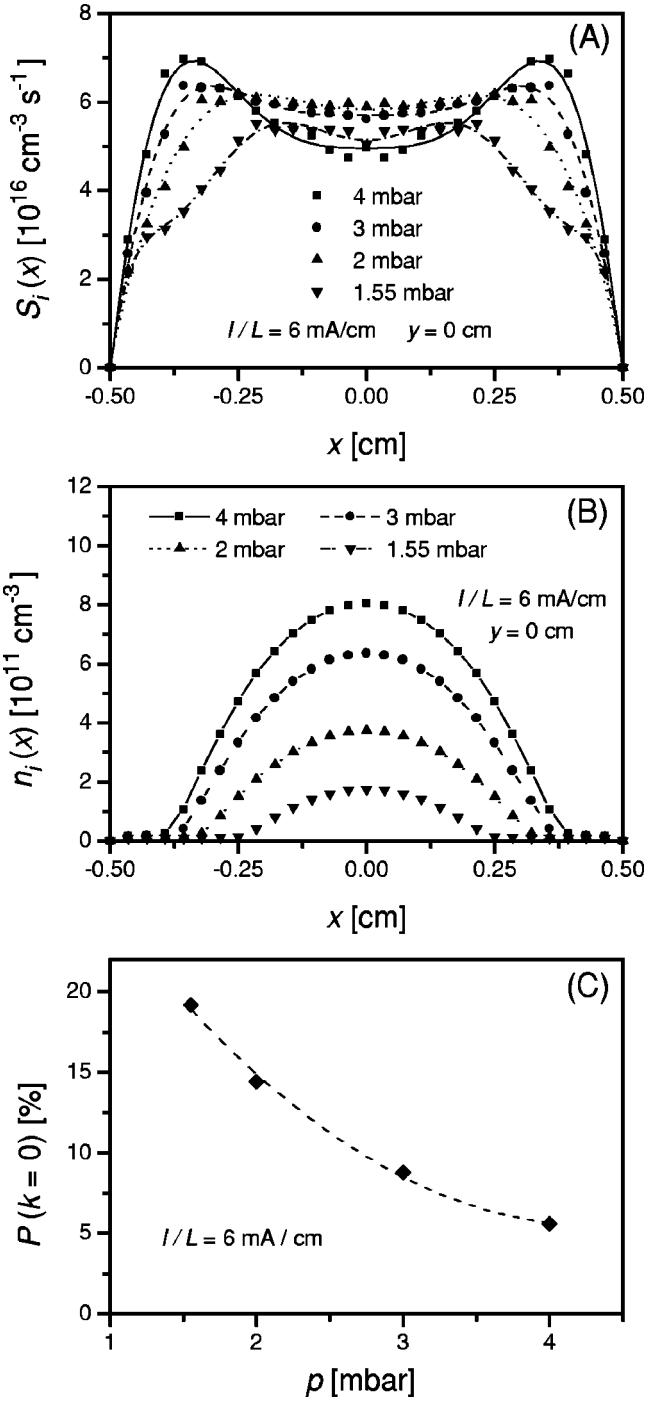

FIG. 11. Ionization source function $S_i(x)$ (a), He^+ density $n_i(x)$ (b) and the probability of producing zero ions in electron avalanches (c) for different values of helium pressure, at constant linear current density of $I/L=6$ mA/cm.

pressure decreases from 4 mbar to 1.55 mbar, although the S_i source function decreases only by 20–30%. This effect can be explained by the increasing rate of losses at lower pressures. The probability that a primary electron is absorbed on the anode surface before producing any ions $[P(k=0)]$ increases drastically with decreasing pressure, as can be seen in Fig. 11(c). This is one of the effects that can explain the gradually increasing slope of the voltage-linear current density curves with decreasing pressure (see Fig. 2).

The difference of the plasma potential (the highest potential in the negative glow) and the anode potential was always found to be 5 – 6 V, independently of the discharge conditions.

C. Effect of the backscattering of fast electrons from the anode

As a high number of fast electrons are absorbed on the anode surfaces, it is expected that their possible backscattering (reflection) into the discharge volume has a significant effect on the discharge parameters. Such effects have already been found to be important in obstructed discharges [43,44].

In the following we present characteristic results of the effect of electron backscattering from the anode. In our calculations we have assumed that the fast electrons (which are traced in the Monte Carlo simulation) are reflected from the anode with a probability independent of the electron energy and angle of incidence. The results are presented for a backscattering coefficient $R=0.2$, with $p=2$ mbar and $V=300$ V. (We use a relatively low value for the backscattering coefficient, for metal electrodes R is expected to be higher. Nevertheless, the value $R=0.2$ already clearly indicates the effects caused by the backscattering of fast electrons from the anodes.)

Figures 12(a) and 12(b) show the ionization source function $S_i(x)$ and the ion density $n_i(x)$ along the X axis of the discharge, respectively, calculated without and including the backscattering of fast electrons from the anode. It can be seen in Fig. 12(a) that the ionization source function is increased by a factor of ≈ 1.5 at $R=0.2$ compared to its value at $R=0$; this increase results from the additional ionization created by the backscattered electrons. Because of the enhanced ionization rate the density of charged particles is also increased. In the center of the discharge the ion density is increased by 90% for the above parameters, see Fig. 12(b). The increase of S_i and n_i is also accompanied by an increase in the linear current density. At $R=0.2$ the linear current density was found to be 4.9 mA/cm for $p=2$ mbar and $V=300$ V, whereas for $R=0$ it was 3.0 mA/cm for the same voltage and pressure. It can also be seen from Fig. 12(b) that there is a reduction in the length of the cathode sheath.

Figure 12(c) shows the $P(k)$ distributions obtained at backscattering coefficients $R=0.2$ and $R=0$. It can also be seen in this figure that the probability of producing $k \leqslant 3$ ions decreased at $R=0.2$ whereas electron avalanches with $4 \leqslant k \leqslant 8$ became more frequent. The probability of producing $k=0$ ions in an electron avalanche decreased to 12% from $P(k=0)=14\%$, found at $R=0$.

D. Comparison with experiment

The only published data obtained for a similar electrode configuration are those of Rocca and Floyd, who investigated the effect of the longitudinal magnetic field on the discharge characteristics [30]. The electrode configuration described in Ref. [30] is similar to our discharge arrangement though the operating conditions are different. Rocca and Floyd's hollow cathode discharge had a rectangular cross section with a cathode to anode surface ratio of 1/2, the width of the cathodes and the anodes was 0.7 and 1.4 cm, respectively, their

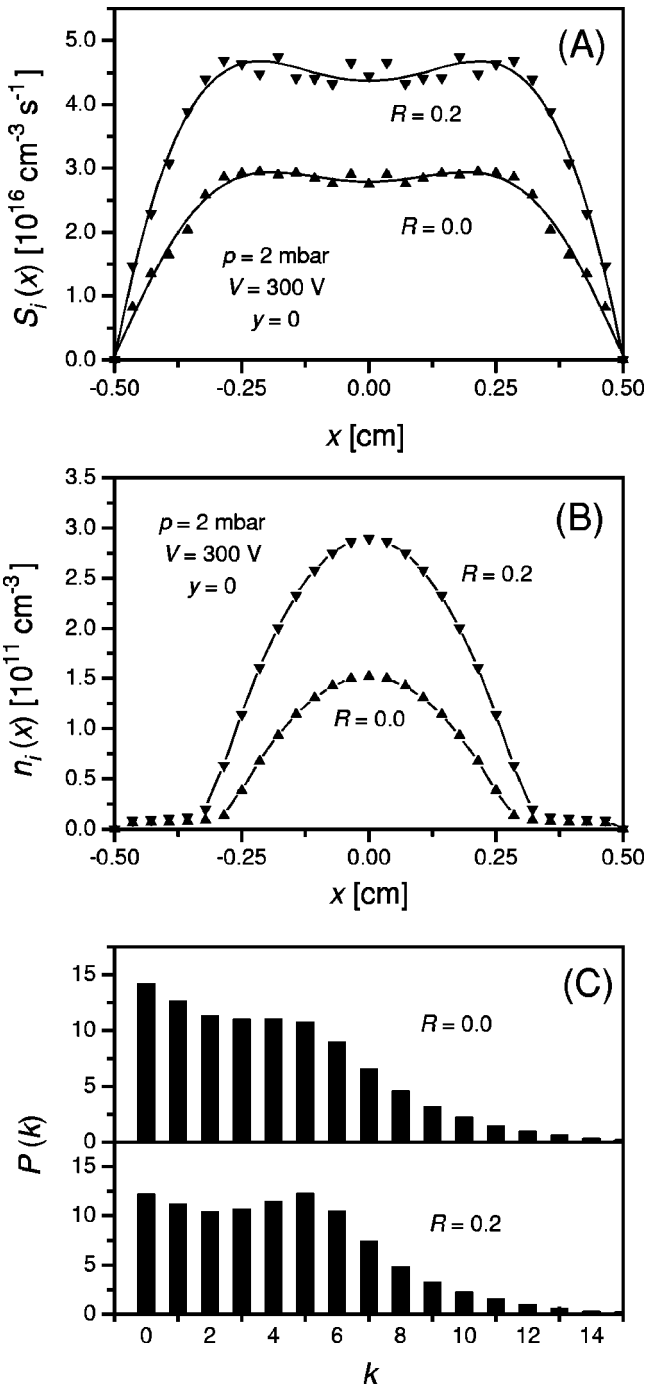

FIG. 12. Effect of backscattering of fast electrons from the anodes on the ionization source function $S_i(x)$ (a) and He^+ density $n_i(x)$ (b). The $P(k)$ distributions obtained at $R=0.2$ and $R=0.0$ (c) ($p=2$ mbar, $V=300$ V).

length was 6 cm. The discharge was operated in dc and pulsed mode. For the dc measurements a 10 kΩ ballast resistor was connected between a stable voltage source and the discharge tube. It was found that a magnetic field in the $B \approx 10$ mT range decreased the discharge current by more than an order of magnitude. The typical operating pressure was in the 1–2 Torr (≈1.3–2.6 mbar) range and the discharge voltage ranged between 1500 and 2000 V. The high operating voltage—being approximately 5 times higher than in our case—was due to the largely increased anode surface where the energetic electrons are absorbed with a much higher probability.

To compare the results of the present model with the experimental data we modified our discharge arrangement in accordance with the dimensions given in [30] and included the external resistor in our simulations. After every time step in the fluid model the anode potential was adjusted according to the value of the discharge current in the previous time step. To study the effect of the longitudinal magnetic field, the fluid equations were solved over one ''half'' of the cross section of the discharge, on a 15×29 grid. The dominant effect of longitudinal magnetic field in this type of discharge arrangement is assumed to be on the motion of fast electrons, which play the main role in maintaining the discharge. Thus the magnetic field was taken into account only in the Monte Carlo simulation of fast electrons.

We could reproduce the electrical characteristics of the discharge (at $B=0$) at a higher pressure than that given in [30]. To achieve $I=30$ mA at 1800 V source voltage (1500 V discharge voltage) the pressure had to be taken as $p \approx 2.9$ mbar instead of the experimental value 2.0 mbar (corresponding to the conditions given in Fig. 2 of Ref. [30]). This difference can be explained as follows:

(1) In the simulations the anodes of the discharge were assumed to absorb the electrons arriving there. The possible backscattering of fast electrons from the anode surfaces is expected to play a more important role in the experiment as the cathode to anode surface ratio was 1/2 in contrast to the symmetrical discharge studied in the model.

(2) At discharge voltages in the 1500–2000 V range the ionization by fast heavy particles may start to play a role in the maintenance of the discharge. Such processes can be excluded in the 200–400 V voltage range.

(3) We neglected gas heating in our calculations. However, under the experimental conditions the electrical input power into unit length of the discharge is significantly higher than for the simulation conditions.

In the simulations the increasing magnetic field resulted in a decrease of the discharge current, in agreement with the experimentally found behavior. However, compared with experiment in our calculations a faster decrease was found (the current $I=30$ mA at $B=0$ decreased to 24 mA in the experiment and to 10 mA in our simulations). We believe that the decrease of current would be less abrupt if we take into account the backscattering of fast electrons from the anodes. In this way the agreement between experiment and the results of calculations could be further improved. We plan to investigate—both theoretically and experimentally—the effect of electron backscattering from the anode on the discharge characteristics.

IV. SUMMARY

We have investigated a rectangular, transverse hollow cathode discharge by means of a two-dimensional self-consistent hybrid model. The high energy electrons were traced by Monte Carlo simulation to provide a fully kinetic

description of their motion. For the slow electrons and for positive ions a fluid model was used, the continuity, the momentum transfer equations, and the Poisson equation were solved using an implicit integration scheme.

The calculations were carried out for a cold-cathode abnormal glow discharge in helium, under stationary conditions, at low pressures (1.55–4 mbar) and moderate ($\approx$1 mA/cm^2) current densities.

It was found that in the central region of the discharge (in the negative glow) a plasma potential approximately 5 – 6 V higher than the anode potential develops. The potential distribution in the cross section of the discharge ensures that the ions produced above the necessary amount to sustain the discharge are directed towards the anode. This results in a significant positive ion flux to the anode (comparable to the ion flux to the cathode).

For the discharge conditions investigated the negative glow of the discharge was found to consist of a quasineutral plasma with typical charged particle concentration in the order of 10^{11} cm^{-3}.

The energy distribution function of electrons absorbed by the anode indicated that a significant number of high-energy electrons are absorbed, which is a major loss for the maintenance of the discharge. It was also found that a number of primary electrons are absorbed by the anode before they could produce any ions. The losses of high-energy electrons at the absorbing anodes and the loss of charges to the anodes from the negative glow explain the increased slope voltage-linear current density characteristics, compared with cylindrical hollow cathode discharges.

The calculations gave evidence for the presence of the hollow cathode effect in the discharge, in the range of operating conditions investigated. The shape of the ionization source function was found to exhibit a characteristic change with decreasing pressure due to the gradually increasing overlap of ionization source functions corresponding to electron avalanches starting from the opposing cathodes.

High-energy electrons backscattered from the anodes resulted in $\approx$90% increase of the He^+ density and $\approx$60% increase of the linear current density for $p=2$ mbar and $V=300$ V, at $R=0.2$.

Comparison of the results of simulations with experimental data showed reasonable agreement. We suggest that if the backscattering of fast electrons from the anodes is considered (and the detailed features of the backscattering process are taken into account) this would enhance the agreement.

ACKNOWLEDGMENTS

I thank A. Bogaerts, L. C. Pitchford, J. P. Boeuf, J. J. Rocca, K. Rózsa, and L. Szalai for helpful discussions, and the Hungarian Science Foundation for supporting this work through OTKA Grant Nos. F-15502 and T-25989.

[1] G. Francis, in *Encyclopedia of Physics* (Springer, Berlin, 1956), Vol. XXII.
[2] P. F. Little and A. von Engel, Proc. R. Soc. London, Ser. A **224**, 209 (1954).
[3] H. Helm, Z. Naturforsch. A **27**, 1812 (1972).
[4] Z. Donkó, Z. Naturforsch. A **48**, 457 (1993).
[5] V. I. Kolobov and L. D. Tsendin, Plasma Sources Sci. Technol. **4**, 551 (1995).
[6] L. C. Pitchford, J. P. Boeuf, P. Segur, and E. Marode, in *Non-equilibrium Effects in Ion and Electron Transport*, edited by J. W. Gallagher (Plenum Press, New York, 1990).
[7] V. I. Kolobov and V. A. Godyak, IEEE Trans. Plasma Sci. **23**, 503 (1995).
[8] Tran Ngoc An, E. Marode, and P. C. Johnson, J. Phys. D **10**, 2317 (1977).
[9] J. P. Boeuf and E. Marode, J. Phys. D **15**, 2169 (1982).
[10] M. Ohuchi and T. Kubota, J. Phys. D **16**, 1705 (1983).
[11] D. A. Doughty, E. A. Den Hartog, and J. E. Lawler, Phys. Rev. Lett. **58**, 2668 (1987).
[12] S. Hashiguchi and M. Hasikuni, Jpn. J. Appl. Phys., Part 1 **27**, 1010 (1988).
[13] M. Yumoto, Y. Kuroda, and T. Sakai, J. Phys. D **24**, 1594 (1991).
[14] Z. Donkó and M. Jánossy, J. Phys. D **25**, 1323 (1992).
[15] J. E. Lawler, Phys. Rev. A **32**, 2977 (1985).
[16] A. C. Dexter, T. Farrell, and M. I. Lees, J. Phys. D **22**, 413 (1989).
[17] N. Sato and H. Tagashira, IEEE Trans. Plasma Sci. **19**, 102 (1991).
[18] M. Surendra, D. B. Graves, and G. M. Jellum, Phys. Rev. A **41**, 1112 (1990).
[19] T. J. Sommerer, M. S. Barnes, J. H. Keller, M. J. McCaughney, and M. J. Kushner, Appl. Phys. Lett. **59**, 638 (1991).
[20] T. J. Sommerer and M. J. Kushner, J. Appl. Phys. **71**, 1654 (1992).
[21] K. H. Schoenbach, H. Chen, and G. Schaefer, J. Appl. Phys. **67**, 154 (1990).
[22] J-H. Tsai and C-H. Wu, J. Phys. D **26**, 496 (1993).
[23] F. Y. Huang and M. J. Kushner, J. Appl. Phys. **78**, 5909 (1995).
[24] J. P. Boeuf and L. C. Pitchford, IEEE Trans. Plasma Sci. **19**, 286 (1991).
[25] A. Fiala, L. C. Pitchford, and J. P. Boeuf, Phys. Rev. E **49**, 5607 (1994).
[26] A. Fiala, Ph.D. thesis, Université Paul Sabatier (1995).
[27] A. Bogaerts, R. Gijbels, and W. J. Goedheer, J. Appl. Phys. **78**, 2233 (1995).
[28] A. Bogaerts and R. Gijbels, J. Appl. Phys. **79**, 1279 (1996).
[29] A. Bogaerts, Ph.D. thesis, University of Antwerp (1996).
[30] J. J. Rocca and K. Floyd, Appl. Phys. Lett. **61**, 901 (1992).
[31] R. C. Tobin, K. A. Peard, G. Bode, K. Rózsa, Z. Donkó, and L. Szalai, IEEE J. Sel. Top. Quantum Electron. **1**, 105 (1995).
[32] J. A. Kunc and W. H. Soon, Phys. Rev. A **43**, 4409 (1991).
[33] E. A. Den Hartog, D. A. Doughty, and J. E. Lawler, Phys. Rev. A **38**, 2471 (1988).
[34] T. J. Sommerer, W. N. G. Hitchon, R. E. P. Harvey, and J. E. Lawler, Phys. Rev. A **43**, 4452 (1991).
[35] F. J. de Heer and R. H. J. Jansen, J. Phys. B **10**, 3741 (1977).

[36] C. Birdsall, IEEE Trans. Plasma Sci. **19**, 65 (1991).
[37] D. P. Lymberopoulos and J. D. Schieber, Phys. Rev. E **50**, 4911 (1994).
[38] S. Yoshida, A. V. Phelps, and L. C. Pitchford, Phys. Rev. A **27**, 2858 (1983).
[39] C. B. Opal, W. K. Peterson, and E. C. Beaty, J. Chem. Phys. **55**, 4100 (1971).
[40] R. Deloche, P. Monchicourt, M. Cheret, and F. Lambert, Phys. Rev. A **13**, 1140 (1976).
[41] A. L. Ward, J. Appl. Phys. **33**, 2789 (1962).
[42] D. L. Scharfetter and H. K. Gummel, IEEE Trans. Electron Devices **16**, 64 (1969).
[43] Z. Donkó, K. Rózsa, R. C. Tobin, and K. A. Peard, Phys. Rev. E **49**, 3283 (1994).
[44] Z. Donkó and K. Rózsa, Acta Phys. Univ. Comenianae **36**, 35 (1995).